Magnetic behavior and structure of compositionally modulated Cu-Ni thin films

E. M. Gyorgy, D. B. McWhan, J. F. Dillon, Jr., L. R. Walker, and J. V. Waszczak
Bell Laboratories, Murray Hill, New Jersey 07974
(Received 30 November 1981)

A series of modulated Cu-Ni films has been prepared with varying wavelength, λ, and amplitude, A, of the compositional modulation. The films have coherent interfaces between the copper and nickel regions over at least the range $16 < \lambda < 120$ Å and several of the films are essentially single crystals containing growth faults. A model for the magnetic behavior based on the assumption that each layer is not significantly different from a random alloy of the same composition agrees with the measurements of the average magnetic moment and the Curie temperature. This suggests the absence of significant two-dimensional effects.

I. INTRODUCTION

The synthesis of chemically modulated metallic films has stimulated the search for anomalies in their physical properties as a function of the modulation.[1] For systems in which one of the constituents is magnetic, the possibility exists of observing a crossover from three- to two-dimensional magnetic behavior with decreasing thickness of the magnetic regions, and a number of papers have focused on the Cu-Ni system.[2–8] Copper and nickel form a continuous solid solution above $T \approx 400\,^{\circ}\mathrm{C}$,[9] and the magnetic properties of the random alloys show a smooth decrease in the magnetic moment and in the Curie temperature with increasing concentration of copper up to $Cu_{0.53}Ni_{0.47}$ which is nonmagnetic.[10] Early studies of chemically modulated films with an average composition near the $Cu_{0.6}Ni_{0.4}$ suggested a large enhancement of the moment of Ni over that of the pure metal at low temperatures.[2] Subsequent studies showed that the average moment was reduced[3–5] and that there was a large in-plane anisotropy.[3,6]

In this paper a more detailed account is given of our earlier measurements,[3] and the observed magnetic properties are compared with a model for chemically modulated films which assumes that the magnetic properties of each atomic layer are not significantly different from those of a random alloy of the same composition. Because Cu and Ni readily interdiffuse, the amplitude A of the chemical modulation (and therefore the average composition per layer) can be varied by changing the modulation wavelength, λ, or by annealing. For short λ, A is less than 100% because of interdiffusion during growth and at a given λ, A can be reduced by annealing. Samples with a range of amplitudes have been prepared by both methods, and comparison with the model suggests that no crossover to two-dimensional magnetic behavior is observed.

In order to determine the modulation amplitude, and to gain insight into the growth of modulated films, a detailed study of the structure and coherence of the films has been made using x-ray diffraction techniques. Previous studies with the scattering vector normal to the film have shown that the films grow with a [111] texture and that the interfaces are coherent at short wavelengths.[11,12] The present studies establish that the Cu-Ni films grow as coherent crystals on the mica substrate with grain sizes exceeding 1000 Å and an average fluctuation in the modulation wavelength through the film of $\Delta\lambda/\lambda \approx 0.05$. Within each grain the structure is coherent, i.e., it can be described by a reciprocal lattice with $\vec{G} = h\vec{a}^* + k\vec{b}^* + l\vec{c}^* \pm m\vec{k}$ where h, k, l, and m are integers, $\vec{a}^*$, $\vec{b}^*$, and $\vec{c}^*$ the average reciprocal-lattice vectors, and $|\vec{k}| = 2\pi/\lambda$ is the wave vector of the modulation. Substantial coherency strains are present in all the samples with λ varying from 16 to 120 Å, i.e., ~ 8 to ~ 60 atomic layers.

This paper has been divided into separate sections on the structural and the magnetic properties and these are presented as Secs. II and III, respectively.

II. STRUCTURE AND COHERENCE

The x-ray measurements were made using a computer controlled three crystal spectrometer equipped with a $\frac{1}{4}$ circle Eulerian cradle. The x-ray source was a Rigaku rotating anode generator operating at 8 kW with a Cu target in the line mode which gives a projected line 0.05×10 mm^2. For the studies of the texture and the determination of the average structure, flat pyrolytic graphite crystals were used for both monochromator and analyzer. For the measurement of the linewidths and also for the samples with longer wavelengths, the resolution was tightened, by using a flat LiF analyzer after the sample and by narrowing the slit before the monochromator. This gave a longitudinal resolution of $\Delta Q = 0.003$ Å^{-1} as determined from the full width at half maximum (FWHM) of the (400) reflection of a GaAs plate.

The samples were prepared by evaporation on a mica substrate as described in Ref. 3. The mechanical shutters over the Cu and Ni evaporation ovens were controlled by thickness monitors to deposit alternating regions of thickness t_{Cu} and t_{Ni} which corresponded to approximately integral numbers of close packed atomic layers of Cu and Ni. The process was continued for N repetitions, and the resulting samples are designated by $[t_{Cu}|t_{Ni}]N$ with the t's in Å (for example [8|8] 3135 designates 3135 repetitions of the bilayer of 8 Å Cu on 8 Å Ni). Each atomic layer is ~ 2.06 Å thick and a modulation wavelength of $\lambda = 16.3$ Å corresponds to ~ 8 atomic layers.

Films of Cu-Ni deposited on mica tend to show [111] texture[11,12] and the initial characterization of the samples was made by rotating the crystal through the (111) reflection and determining the FWHM of the rocking curve. The samples seemed to fall into two classes, those with rocking curves of $> 15°$ and those with rocking curves in the range 1–6°. Only samples in the latter class were used for further x-ray or magnetic measurements. The samples and their FWHM are listed in Table I. The reason for the large differences in the rocking curve width is not known and an exhaustive study has not been made. There appears to be a dependence on growth rate as illustrated by the two [20|10] samples listed in Table I. They were grown on successive days under identical conditions except that the growth rates were 2 and 5 Å/sec for the [20|10] samples with FWHM of 1.4 and 15°, respectively.

For more detailed structural studies several samples were removed from the mica substrates by gluing them to glass cover slips and then peeling off the mica. In addition, for the [8|8] and [30|30] samples, the 2000-Å layer of copper was preferentially etched away using a dilute solution of chromic acid. Several samples were also studied after annealing between copper blocks in vacuum for various periods of time at $T = 400$ or 440 °C.

Pure copper and nickel are face-centered cubic with lattice parameters at room temperature $a_{Cu} = 3.6150$ Å and $a_{Ni} = 3.5239$ Å. In a stereographic projection for [111] texture, Fig. 1(a), the grains have [111] perpendicular to the substrate and $[1\bar{1}0]$ and $[11\bar{2}]$ parallel to the substrate. For convenience a hexagonal unit cell can be defined, and the reciprocal lattice corresponding to the $(H0.L)$ scattering plane is shown in Fig. 1(b). The large closed circles represent the average lattice and the smaller closed circles the satellites resulting from the chemical modulation along $[00.L]_{hex}$. The stereographic projection shows threefold symmetry along $[00.L]$ because the structure is rhombohedral. If there are stacking growth faults, then the macroscopic symmetry will be sixfold because the reciprocal lattice on one side of the growth fault is rotated by 60° around $[00.L]$ from that on the other side. If there is a random distribution of growth faults, then the $(H0.L)$ plane will contain points of equal intensity from each lattice as shown in Fig. 1(b) by the open and closed circles. This is illustrated for the [8|8] sample in Fig. 2 by a scan along $[10.L]$. The (10.2) from one orientation and the $(\bar{1}0.1)$ from another are clearly seen along with the $m = -1$ satellites. The macroscopic sixfold symmetry of the film was also confirmed by rotating the sample around [111] and observing that there were $(2\bar{2}0)$ type reflections every 60°.

As the lattice parameters of Cu and Ni differ by 2.5%, the parameters of Cu in the plane will have to compress and those of Ni expand in order to form a coherent interface. It is believed that the resulting coherency strain can only be sustained at fairly short

TABLE I. Sample characterization.

$t_{Cu}\|t_{Ni}$	N	FWHM (deg)	$\langle m \rangle^a / m_1^r$	λ (Å)	A_1	ϵ_1
6|6	2498	7.1	3.3	· · ·		
8|8	3135	0.4	7.7	16.3	0.33	0.028
10|10	2440	6.4	16.0	21.0		
16|16	494	1.5	6.1	31.9	0.4	0.024
	Annealed 400 °C, 12.5 h				0.25	0.016
	Annealed 440 °C, 12.5 h				0.05–0.1	
30|30	303	3.5	6.4	61.8	(0.5)	0.038
60|60	145	2.8	8.9	122.0	(0.5)	> 0.032
20|10	880	1.4	10			
20|10	342	> 15°	5.5			
40|10	800	2.1	13			

[a]Ratio of the magnetization with $\vec{H}$ parallel to the remanent magnetization with $\vec{H}$ perpendicular.

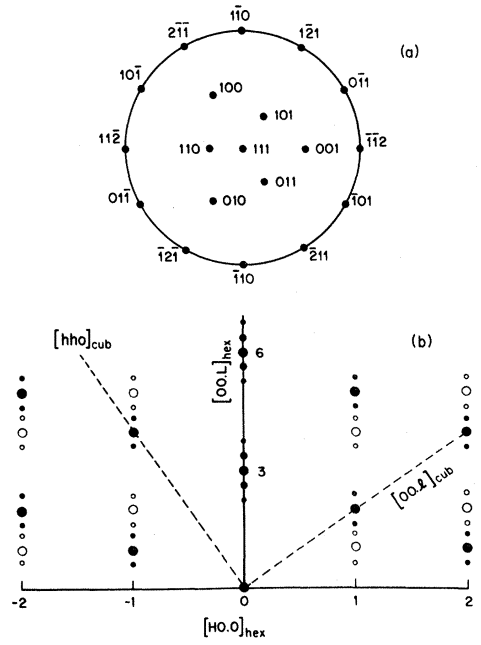

FIG. 1. (a) Stereographic projection for [111] orientation. (b) Reciprocal lattice for a CuNi modulated film containing random growth faults. The two orientations are illustrated by open and closed circles.

modulation wavelength, λ, and that with increasing λ the strain is relieved by the formation of misfit dislocations.[1] The presence of coherent interfaces can be determined by two methods. First the d spacings both in the plane of the film and along the growth direction should be approximately the average of the Cu and Ni lattice d spacings. As the concentration of misfit dislocations increases, the width of the reflections with $\vec{Q}$ in the plane of the film should increase and finally split into two reflections corresponding to pure Cu and pure Ni. Figure 3 compares scans through the $(2\bar{2}0)$ of the [8|8] and [30|30] samples, and a single average peak is observed in both samples. In Table II the ratio of the lattice parameters obtained from the (111) and (222) and from the $(2\bar{2}0)$ reflections are listed for the [8|8] and [30|30] samples. Within experimental error the ratio is unity and the FWHM of the $(2\bar{2}0)$ is similar to that of the (222). A single average lattice exists suggesting that the coherence of the interfaces is not substantially changed even for $\lambda \approx 60$ Å.

The second indication of the presence of coherency strains comes from an analysis of the intensity of the harmonics around the Bragg reflections, and this is coupled with the determination of the composition profile. The evolution of the harmonics around the (111) and (222) reflections with increasing λ is shown for the [8|8] and [30|30] samples in Fig. 4 and for the [60|60] sample in Fig. 5. All these measurements were taken using tight resolution. The Cu buffer layer was not removed from the [60|60] sample, and the reflections from the Cu buffer layer, which were superimposed on the multilayer data, are indicated in the figure by the shading. As expected, with increasing λ the harmonics move closer to the Bragg reflections and they grow in intensity at the expense of the Bragg peak until in the [60|60] sample the harmonics around (222) are stronger than the (222) reflection. The peak to background ratio decreases rapidly with increasing width of the rocking curve so that it is difficult to observe harmonics much above the third or fourth even in the [60|60] sample which should have a composition profile approaching a square wave.

In order to obtain the first Fourier coefficient of the composition wave and the leading term in the interplanar spacing modulation, the Bessel function expansion up to second order, given by Segmüller and Blakeslee,[13] was used. The integrated intensities of the harmonics for the [8|8] and [30|30] samples were corrected for Lorentz-polarization, absorption, and Debye-Waller factors as described in Ref. 14 and normalized to the parent Bragg peak. The ratio of the observed structure factors are listed in Table II. In

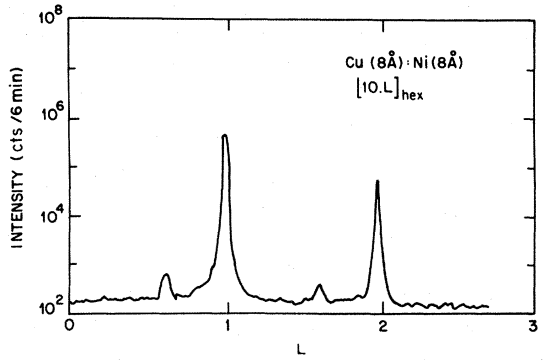

FIG. 2. Scan along $[10.L]_{hex}$ showing that the film is best characterized as a single crystal containing a random distribution of growth faults.

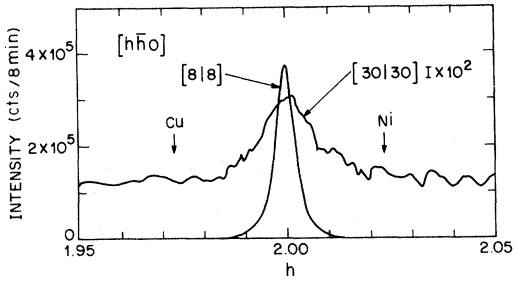

FIG. 3. Comparison of scans through the $(2\bar{2}0)$ for the [8|8] and [30|30] films showing that a single average reflection is observed indicating the presence of coherent interfaces. The positions of the reflections for pure Cu and Ni are shown.

TABLE II. Calculated and observed structure factors.

		[8|8]3135			[30|30]303		
		FWHM	$\|F_m\|/\|F(hkl)\|$		FWHM	$\|F_m\|/\|F(hkl)\|$	
(hkl)	m	(Å^{-1})[a]	Obs.	Calc.	(Å^{-1})[a]	Obs.	Calc.
	+1		0.006	0.005			
(000)	+2		0.001	−0.001			
	+3		0.002				
	−2	0.044	0.008	−0.009		0.06	0.06
	−1	0.023	0.066	0.070	0.016	0.27	0.31
(111)		0.009			0.013		
	+1	0.022	0.047	−0.044	0.019	0.29	−0.27
	+2		0.006	0.006		0.05	0.04
	−2		0.013	0.013		0.28	0.23
	−1	0.028	0.134	0.135	0.035	0.66	0.69
(222)		0.018			0.032		
	+1	0.029	0.094	0.095	0.038	0.64	−0.63
	+2					0.20	0.17
$(2\bar{2}0)$		0.019			0.042		
$a(111)/a(2\bar{2}0)$		1.0013			1.0007		
A_1				0.33			(0.5)
A_2				−0.09			(+0.1)
ϵ_1				0.028			0.038
ϵ_2				−0.004			(+0.002)

[a]Instrumental resolution $=0.003$ Å^{-1}.

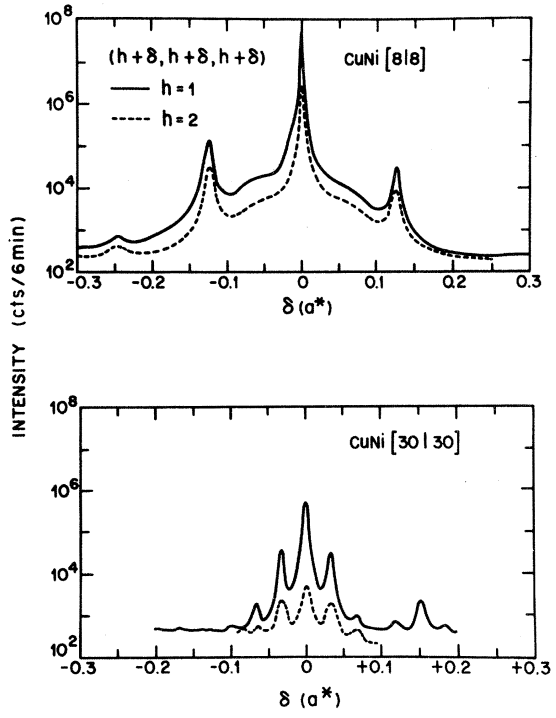

FIG. 4. Scans along [111] through the (111) and (222) for the [8|8] and [30|30] samples. Note presence of (200) and its satellites at $\delta=+0.15$ for the [30|30] sample which indicates some loss of texture.

the model of Segmüller and Blakeslee the composition and interplanar spacing modulation are given along the growth direction by

$$C_{\mathrm{Ni}}(z)=C_{\mathrm{av}}+A_1\cos kz+A_2\cos 2kz\ ,$$

$$D(z)=d_{\mathrm{av}}(1+\tfrac{1}{2}\epsilon_1\cos kz+\tfrac{1}{2}\epsilon_2\cos 2kz)\ ,$$

where $k=2\pi/\lambda$. For our samples $C_{\mathrm{av}}=0.5$ and A_1 can vary from 0 for a random alloy to $2/\pi$ for a square wave. The atomic scattering factors needed in the intensity calculations were taken from Ref. 15 and they included the real part of the dispersion correction. The results of a detailed fit to the observed data for the [8|8] and [30|30] samples are shown in Table II and values of A_1 and $\epsilon_1/2$ obtained for several samples are listed in Table I. The overall fit is reasonably good for the [8|8] sample which has a rocking curve of 0.4°. It should be pointed out that with increasing λ, the A_1 and ϵ_2 parameters are highly correlated. The average magnitude of the −1 and +1 harmonics is mainly determined by ϵ_1 and therefore the error in this parameter is ±5%. The difference in structure factor between the −1 and +1 harmonics comes from a competition between the leading strain term (ϵ_1) and the leading term in the scattering power modulation (A_1). However this difference is partially offset by the contributions to the first harmonic from higher-order Bessel functions times ϵ_2. As a result the values of A_1 and ϵ_2 are correlated for the samples with longer wavelengths,

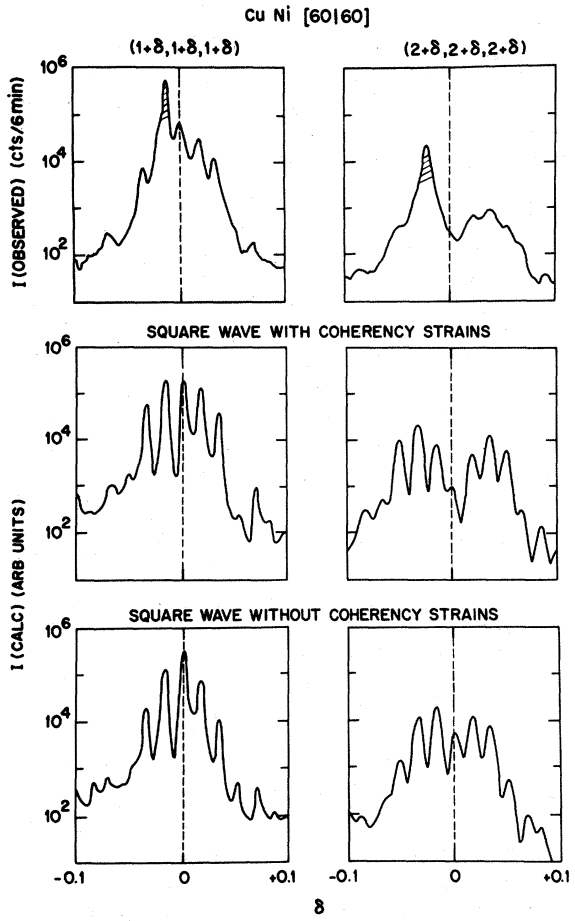

FIG. 5. Comparison of scans through the (111) and (222) reflections for the [60|60] with model calculations assuming coherent and incoherent interfaces. The shaded peak, which is the highest in each of the top figures, results from the Cu buffer layer.

and the data are consistent with $A_1 \sim 0.5$. As can be seen in Table I, A_1 increases with increasing λ and decreases with annealing. This is consistent with not having a full chemical modulation at short wavelengths because of interdiffusion and with full modulation and thick interfaces at long wavelengths.

All the values of ϵ_1 in Table I are consistent with the interfaces being coherent. If there are coherent interfaces, then the (111) planes of the Cu contract in the plane of the film and the (111) planes of the Ni expand so that there is a single average lattice parameter in the plane of the film. The resulting coherency strain causes a strain of opposite sign perpendicular to the film as expected from Poisson's ratio. The appropriate combination of elastic constants leads to an increase in the interplanar spacing modulation along the growth direction to $\epsilon_1 = 0.038$.[1,12] If the coherency strains were relieved by misfit dislocations then ϵ_1 would just be the difference in the interplanar spacing of the pure elements, i.e., 0.025. The values of ϵ_1 in Table I are closer to the coherent values at long λ. At shorter λ the values are consistent with the scaling of ϵ_1 by the fractional decrease in the chemical modulation.

In addition to the determination of the orientation and structure of the grains in the Cu-Ni modulated films, the x-ray measurements provide information about the size of the grains and the fluctuations in the average d spacing and in the modulation wavelength. The FWHM of the reflections is listed in Table II. The (222) reflection is almost twice as wide as the (111) and the width of the harmonics increases approximately linearly with the order of the harmonic, i.e., $\Delta Q/Q$ and $\Delta q/q = \text{const}$, where Q is the scattering vector of the average lattice, $q = mk$ is the wave vector of the mth harmonic, and ΔQ and Δq are the FWHM of the Bragg reflections and of the harmonics, respectively. This implies that there is a range of average d spacings and of modulation wavelengths given by $\Delta Q/Q = \Delta d/d$ and $\Delta q/q = \Delta\lambda/\lambda$, respectively. For the [8|8] sample $\Delta d/d = 0.03$ and $\Delta\lambda/\lambda = 0.05$ showing that the deposition technique for these modulated films is reasonably uniform.

In order to make a more realistic comparison with the data for the [60|60] sample and to account for the diffuse scattering observed under the Bragg peaks in the [8|8] sample, a computer program was written to calculate the intensity as a function of scattering vector along the growth direction. The model included (1) a Fourier cosine series for the composition modulation of up to 25 terms and a corresponding sine series for the displacements of the ions from their average position, (2) a variable number of coherently stacked layers up to 900, (3) a Gaussian distribution of both λ and d_{av}, and (4) all the appropriate Lorentz, polarization, absorption and Debye-Waller and atomic scattering factors. In the absence of any modulation, the variation in $I(Q)$ vs Q as a function of the average grain size (number of coherently stacked layers) is shown in Fig. 6. This is the standard scattering function $\sin^2 N\phi/\sin^2\phi$ which has a central peak and many weak side bands. For clarity the side bands have been averaged for the two lower curves. Comparison of this figure with the data for the [8|8] sample shows that a grain size of the order of 500 layers could account for most of the diffuse background and this gives an estimate of the lower limit for the average grain size in the growth direction. Another possible cause of diffuse scattering is clustering of Cu or Ni in the close-packed layers. If the clustering were confined to the interfacial regions then rods of diffuse scattering would result. The width of the rods would reflect the average size of the clusters in the plane, and the variation in intensity perpendicular to the layers would reflect the thickness of the clusters. As a simple grain size model can account for most of the diffuse scattering, there

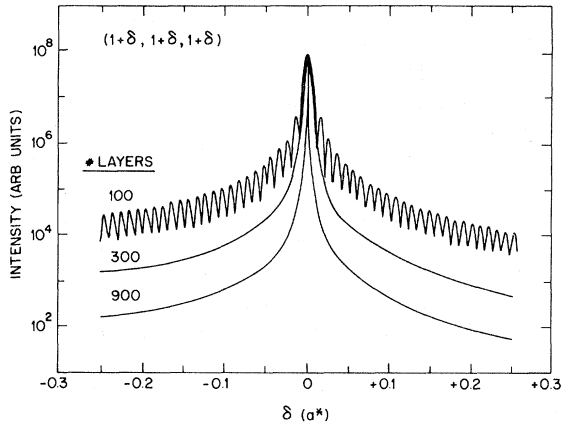

FIG. 6. Calculated intensity vs δ through the (111) reflection as a function of grain size or number of coherently stacked layers. The sidebands have been averaged in the lower two curves. Comparison with Fig. 4 suggests a grain size ~700 Å for the [8|8] sample.

is no need to invoke a complicated clustering model. We are only able to set a lower limit of the grain size in the plane of the film. If it is assumed that the main contribution to the width of the $(2\bar{2}0)$ reflection comes from finite particle size effects then a lower limit of ~300 Å is obtained for the [8|8] sample. However, as indicated above, most of the broadening of the reflections along the growth direction can be attributed to fluctuations in the average d spacing. It is likely that similar effects dominate the linewidth of the in-plane reflections and that the average grain size in the plane is much greater than 300 Å. A comparison of the model calculations with the observed data for the [60|60] sample is shown in Fig. 5. The assumed parameters were a coherent stacking of 250 layers, $\Delta d/d = 0.002$ and $\Delta\lambda/\lambda = 0.03$. A square wave was assumed and the values of the displacement terms assumed $\epsilon_n = A_n\epsilon_0$ where ϵ_0 was either 0.025 or 0.038 for incoherent and coherent interfaces. After mentally subtracting the peaks from the Cu buffer layer, it is seen that the agreement is better in the limit of coherent interfaces in agreement with our earlier analysis.

III. MAGNETIC BEHAVIOR

The magnetic results reported here are an extension of the preliminary results given in Ref. 3. The main points made in Ref. 3 were that the magnetic moment is less than that of pure Ni and that this moment decreases with decreasing thickness of the Ni layers. Furthermore, it was shown that these modulated films have a large surface anisotropy that tends to keep the magnetization in the plane of the film. In fact, it was the assumption that this surface anisotropy was negligible that led to the early erroneous report that these films had an enhanced moment.[2]

With the more extensive x-ray data presented in the preceding section, a more detailed analysis of the magnetic behavior is now possible. The discussion will be primarily limited to the films for which the modulation amplitude, A_1, is available (Table I). In Fig. 7, we plot the average magnetization, $\langle 4\pi M\rangle$, as a function of A_1 at 4.2 K. The measurements were made with a vibrating sample magnetometer. The applied field was in the plane of the sample. Here and in what follows the moment is defined in terms of the volume of Ni present and not the total volume. With the possible exception of the behavior near small values of A_1, the data in Fig. 7 are in very good agreement with that given in Ref. 5.

Obtaining the value of the magnetization from the low-temperature magnetization (M) versus applied-field (H) data is quite straightforward since the magnetization is essentially saturated in fields less than 1 kG and the extrapolation of the linear M vs H data back to zero field to obtain $\langle 4\pi M\rangle$ is unambiguous.[3,5] However, to determine the Curie temperature (T_c) requires a more detailed analysis of the data. Even for a material with a homogeneous composition, the dependence of M on the applied field causes some difficulty in the determination of T_c.[16,17] This problem becomes even more severe for compositionally modulated films. To begin the discussion of the Curie temperature of modulated samples we will consider a simple model in which $C_{\mathrm{Ni}}(z)$, the fraction of Ni, is adequately described by C_{av} and only the first harmonic, $A_1\cos kz$. We will also initially assume that there is no exchange interaction arising from the

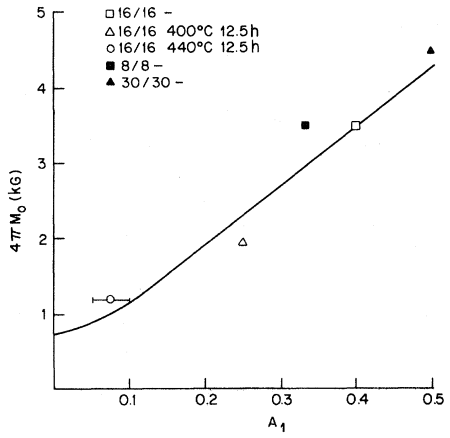

FIG. 7. Average magnetization at 4.2 K as a function of the modulation amplitude. The solid line is calculated from a simple model described in the text.

variation of M with z. This is obviously an oversimplification for very thin films, but still this very simple model allows us to illustrate some of the relevant points that must be considered in the determinations of T_c. The magnetization at $T=0$ is then given by

$$M_0(z)=M_{\mathrm{Ni}}\left[\frac{C_{\mathrm{Ni}}(z)-C_0}{1-C_0}\right],$$

where M_{Ni} is the magnetization of Ni at $T=0$ and C_0 is the critical Ni concentration at which the alloy becomes magnetic. Here we have used the linear dependence of M on C_{Ni} given in Ref. 10. A similar equation gives the variation of T_c with z. To obtain the magnetization as a function of temperature we use the Weiss equation.[16]

$$\frac{M(z,T)}{M_0(z)}=\tanh\left[\frac{M(z,T)/M_0(z)-H/NM_0(z)}{T/T_c}\right],$$

where N is the molecular-field constant and H the applied field. The dependence of $\langle 4\pi M\rangle$ on temperature is obtained by solving this transcendental equation and then integrating over the wavelength.[18] This calculation shows that even in the absence of an applied field the approach of $\langle 4\pi M\rangle$ to zero as the Curie temperature is reached is quite gradual for modulated structures. In contrast, for a uniform alloy with no applied field the Weiss equation gives an infinite slope as M approaches zero at T_c. However, as was stated earlier even for a uniform alloy the presence of an applied magnetic field causes the disappearance of M at T_c not to be perfectly sharp. A common method employed to overcome this problem in experimentally determining the onset of ferromagnetism is to plot M^2 in the vicinity of T_c, as a function of H/M with the temperature as a parameter (Arrott plot).[19] For a homogeneous sample, the temperature at which this plot has a zero intercept is T_c. This conclusion can be readily obtained by expanding the Weiss equation in the region where $M/M_0 \ll 1$.

A priori it is not clear what the significance of an Arrott plot is for compositionally modulated films. Calculations with our simple model show that M^2 depends nearly linearly on H/M and that the Curie temperature deduced from the zero intercept criterion is about 4% lower than the Curie temperature of the region with the highest Ni concentration.[18] Since exchange effects are neglected, these results are, of course, independent of the modulation wavelength.

In order to study the influence of the wavelength on T_c, it is necessary to include exchange effects in the preceding model. To do so we consider discrete atomic layers perpendicular to the film normal. For the ith layer the Weiss equation is

$$\frac{M_i}{M_{0i}}=\tanh\left[\mu_A\left[\frac{H+\frac{1}{2}N[M_i+F(M_{i+1}+M_{i-1})]}{kT}\right]\right],$$

where μ_A is magnetic moment per Ni atom. The meanings of N and M_{0i} are as before with the exception that here M_{0i} is defined only at discrete values of z. The constant F is set equal to $\frac{1}{2}$ to reflect the fact that the number of nearest neighbors in these planes is 3 while there are six nearest neighbors in the ith plane. These coupled, nonlinear equations are solved with the aid of a computer and then summed to obtain $\langle 4\pi M\rangle$ as a function of T and H.

This calculation shows that in this case the Arrott plots are more nearly linear. The T_c determined from these plots is within one degree of that calculated from the disappearance of the magnetization. In contrast to the previous calculation which neglected exchange effects, the calculated temperature at which $\langle 4\pi M\rangle$ disappears may now be, depending on the wavelength, substantially less than the T_c of the Ni-rich region. The calculated values of T_c as a function of A_1, with the Ni thickness as a parameter, are shown in Fig. 8. As might be expected, at a constant modulation amplitude, T_c decreases with t_{Ni}, and at $A_1=0$ the Curie temperature is equal to that of the homogeneous 50at.%-50at.% alloy. The curve with $t_{\mathrm{Ni}}\rightarrow\infty$ is the same as that obtained from the model that neglects exchange.

Both models give that $\langle 4\pi M\rangle$, at $T=0$, is just the average of $M_0(z)$ or M_{0i} over one wavelength. This average is wavelength independent and is a function of A_1 only. For only a small number of layers (less than 3) the atomic layer model gives unrealistic

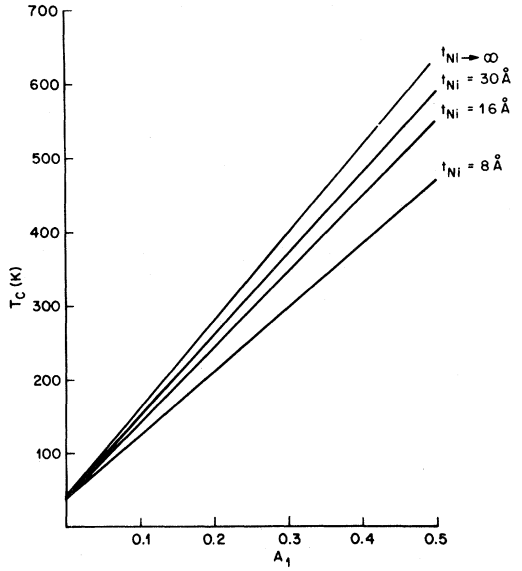

FIG. 8. Curie temperature for four Ni thicknesses as a function of the modulation amplitude. The results are calculated from the model that includes exchange effects which is described in the text.

results due to the discrete nature of M_{0l}. The solid line in Fig. 7 is this average of $M_0(z)$. The curvature at small values of A_1 results from the fact that the homogeneous alloy ($A_1=0$) is magnetic. Thus, with decreasing A_1 there is a relatively sudden increase at $A_1 \sim 0.1$ in the size of the magnetic regions. From Fig. 7 it may be seen that these simple models give a quite accurate description of the experimental low-temperature magnetic behavior.

Examples of magnetic data from which T_c is deduced are shown in Fig. 9 where $\langle M \rangle$ is shown as a function of the applied field at three temperatures in the vicinity of T_c. The sample was the [16|16] film with $A_1=0.4$. Plotted in this fashion the value of T_c is not obvious. In fact, the extrapolation of $\langle M \rangle$ back to $H=0$ would imply $T_c > 455$ K. However, if $\langle M \rangle^2$ is plotted versus $H/\langle M \rangle$ as shown in Fig. 10, the Curie temperature, as defined by this Arrott plot, is unambiguously between 440 and 445 K. The values of T_c obtained in this way are shown in Fig. 11 as a function of A_1. The solid line is the T_c predicted by the model that neglects exchange effects, that is, essentially the Curie temperature of the region with the highest Ni concentration. Since the T_c calculated by the model including exchange depends both on A_1 and λ, the prediction of this model is given by the appropriate calculated points as indicated in the figure. The model including exchange is presumably a better description of the compositionally modulated films, and while the experimental scatter is large, this model indeed appears to give a better fit to the experimental data. The most obvious conclusion to be drawn from Fig. 11, is that

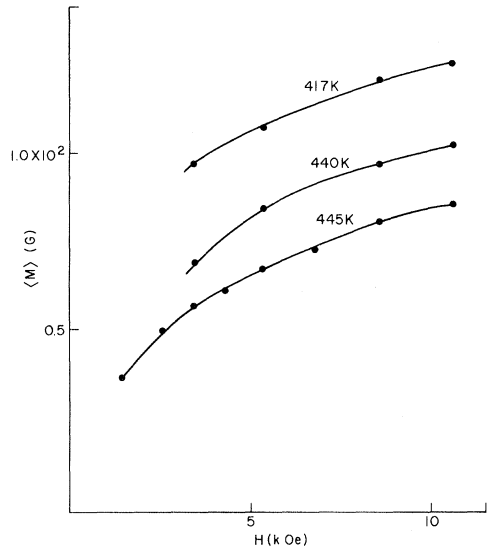

FIG. 9. Magnetization of a [16|16] film with $A_1=0.4$ as a function of the applied field. The three temperatures shown are in the vicinity of T_c.

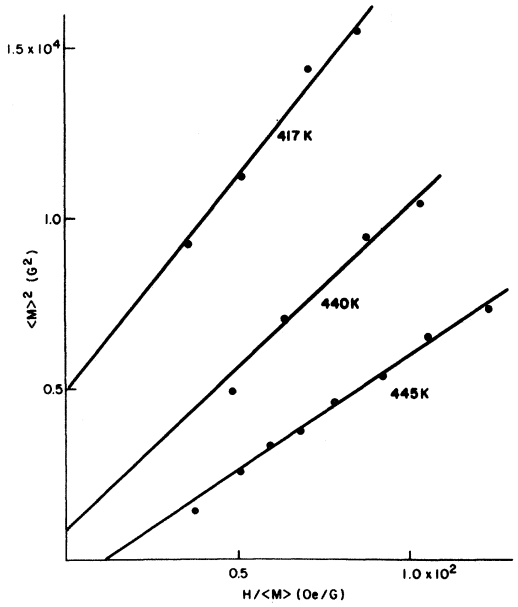

FIG. 10. Same data shown in Fig. 9 plotted here as $\langle M \rangle^2$ as a function of $H/\langle M \rangle$ with temperature as a parameter [Arrott plot (Ref. 19)].

the measured T_c and the calculated T_c both decrease with decreasing A_1. This not unexpected conclusion is in total disagreement with the results given in Ref. 5, where it is reported that T_c is independent of A_1. In Ref. 5 this independence of T_c on A_1 is attributed to the presence of clusters which x-ray results show

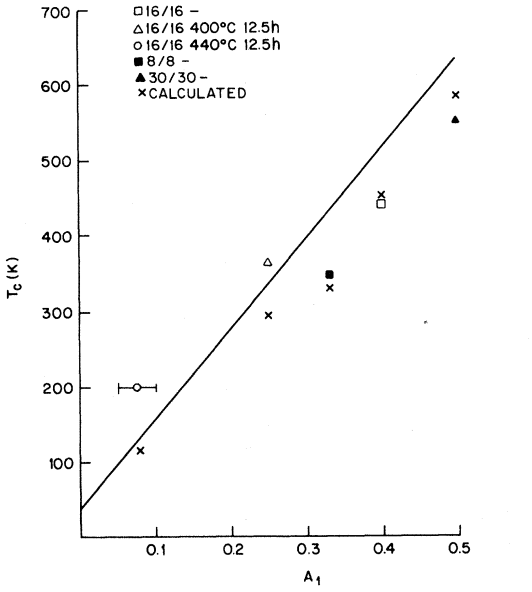

FIG. 11. Curie temperature as a function of the modulation amplitude. The solid line is from a model that neglects exchange. The indicated calculated points are from a model that includes exchanges.

are absent in our films. In this connection it should be noted that the explanation of the magnetic behavior inferred from polarized neutron diffraction also invoked the presence of clusters,[4] and thus these results are not directly applicable to our films.

In summary, the experimentally measured average magnetization at low temperatures and the Curie temperature are fairly well accounted for by the simple models proposed here. Since the low-temperature predictions of these models depend only on A_1 and not on the wavelength or any other modulation effects, the success of these models suggests that these effects are not important. Thus, it is somewhat surprising that thin-film or two-dimensional effects do not appear to be present even down to a Ni thickness of 8 Å, only four atomic layers. This observation is in apparent disagreement with the energy-band calculation of Jarlborg and Freeman,[7] who calculated that the average magnetization of a [6|6] film would be reduced to 0.7 of that of bulk Ni. However, it must be remembered that the energy-band calculation is for a square-wave modulation, that is three distinct layers of Ni and three of Cu whereas our data and models apply to a sinusoidal modulation. It is not clear what an energy-band calculation would give for a sinusoidal modulation and a square-wave modulation is experimentally unattainable. Consequently this apparent discrepancy cannot be resolved at present except to note that for a film as thin as the one studied by Jarlborg and Freeman the reduction in moment is not very large and would be expected to be even smaller for the thicker films experimentally investigated. The value of T_c predicted from the model that includes exchange tends to the value obtained from the wavelength-independent model as A_1 approaches zero or as λ becomes large. Thus, to observe appreciable effects from the thin-film nature of the samples would require films with small wavelengths and large modulation amplitudes. Obviously, these films are the most difficult to fabricate. The Curie temperature for the films actually available (Fig. 11) are not expected to and do not show a very significant dependence on wavelength. As a result, these data cannot be used to discuss the dependence, if any, of T_c on λ. It should be noted, however, that for a fixed t_{Ni} (10 Å) the Curie temperature does not depend on t_{Cu}(10, 20, 40 Å).

ACKNOWLEDGMENTS

We wish to thank B. C. Chambers for assistance in some of the computer calculations and W. R. Jones for permission to use some of his unpublished data.

[1]J. E. Hillard, in *Modulated Structures,* edited by J. M. Cowley, J. B. Cohen, M. B. Salamon, and B. J. Weunsch (American Institute of Physics, New York, 1979), p. 407.
[2]B. J. Thaler, J. B. Ketterson, and J. F. Hilliard, Phys. Rev. Lett. 41, 336 (1978).
[3]E. M. Gyorgy, J. F. Dillon, Jr., D. B. McWhan, L. W. Rupp, Jr., L. R. Testardi, and P. J. Flanders, Phys. Rev. Lett. 45, 57 (1980).
[4]G. P. Felcher, J. W. Cable, J. Q. Zheng, J. B. Ketterson, and J. E. Hilliard, J. Magn. Magn. Mater. 21, L198 (1980).
[5]J. Q. Zheng, C. M. Falco, J. B. Ketterson, and I. K. Schuller, Appl. Phys. Lett. 38, 424 (1981).
[6]J. F. Dillon, Jr., E. M. Gyorgy, L. W. Rupp, Jr., Y. Yafet, and L. R. Testardi, J. Appl. Phys. 52, 2256 (1981).
[7]T. Jarlborg and A. J. Freeman, Phys. Rev. Lett. 45, 653 (1980).
[8]R. M. White and C. Herring, Phys. Rev. B 22, 1465 (1980).
[9]J. Vrijen and S. Radelaar, Phys. Rev. B 17, 409 (1978).
[10]S. A. Ahem, M. J. C. Martin, and W. Sucksmith, Proc. R. Soc. London 248, 145 (1958).
[11]A. J. Purdes, Ph.D. thesis (Northwestern University, 1976) (unpublished).
[12]T. Tsakalakos, Ph.D. thesis (Northwestern University, 1977) (unpublished).
[13]A. Segmüller and A. E. Blakeslee, J. Appl. Crystallogr. 6, 19 (1973).
[14]R. M. Fleming, D. B. McWhan, A. C. Gossard, W. Wiegmann, and R. A. Logan, J. Appl. Phys. 51, 357 (1979).
[15]*International Tables for X-ray Crystallography* (Kynoch, Birmingham, 1976), Vol. IV.
[16]R. M. Bozorth, *Ferromagnetism* (Van Nostrand, Princeton, 1963), Chap. 14.
[17]K. P. Belov, *Magnetic Transitions* (Consultants Bureau, New York, 1961), Chap. 3.
[18]W. R. Jones (unpublished).
[19]A. Arrott, Phys. Rev. 108, 1394 (1957).